LES and unsteady RANS of boundary-layer transition induced by periodically passing wakes

By F. E. Ham†, F. S. Lien†, X. Wu, M. Wang, AND P. Durbin

Results from 3-dimensional large-eddy simulation (LES) and 2-dimensional unsteady Reynolds-averaged Navier-Stokes (RANS) simulation of a spatially-evolving flat-plate boundary-layer undergoing transition induced by periodically passing wakes are presented and compared. The LES simulations used a novel kinetic-energy conserving finite-volume discretization of the incompressible Navier-Stokes equations and the standard dynamic Smagorinsky subgrid-scale model. RANS simulations were based on the STREAM code of Lien & Leschziner (1994) with the $v^2 - f$ turbulence model of Lien & Durbin (1996).

When compared to the direct numerical simulation (DNS) of Wu *et al.* (1999), the LES was able to correctly predict the onset of transition. Inspection of the instantaneous flow field in the transition region confirmed that intermittent turbulent spots were being distinctly resolved. A close inspection of the fluctuating velocities near the top of the boundary layer just prior to spot formation confirmed the presence of the "backward jet" inflectional velocity profile proposed by Wu *et al.* (1999) and Jacobs & Durbin (2000) as the precursor to turbulent spot formation, suggesting that the LES is actually capturing the bypass transition mechanism, at least in these initial stages. The transition length predicted by LES, however, was consistently shorter than the DNS result.

The unsteady RANS simulations were also able to correctly predict the onset of transition, in this case by the mechanism of turbulent diffusion from the turbulence kinetic energy of the passing wake into the boundary layer. The transition length predicted by RANS is also in agreement with the DNS; however, the overshoot of average skin friction relative to the flat plate correlation (seen in both the DNS and present LES) was not observed.

1. Introduction

In orderly transition to turbulence, small disturbances in the laminar boundary layer lead to 2-dimensional Tollmien-Schlichting waves that are amplified through various stages leading eventually to a fully turbulent boundary layer. This relatively slow transition process has been extensively studied in relation to flow over aircraft wings, where the free-stream turbulence levels are generally low (Mayle 1991).

In the presence of disturbances external to the boundary layer, however, it is observed experimentally that transition can occur rapidly, "bypassing" the orderly route. Bypass transition is the dominant mode of transition in many turbomachinery applications, where free-stream turbulence intensities are usually well above the threshold level of about 0.5% (Yang *et al.* 1994). Furthermore, when the dominant free-stream disturbances are periodic in time, such as the periodically passing wakes generated by an upstream row of rotors or stators in a turbine cascade, the transition can also become periodic. In

† University of Waterloo, Waterloo, Ontario, Canada

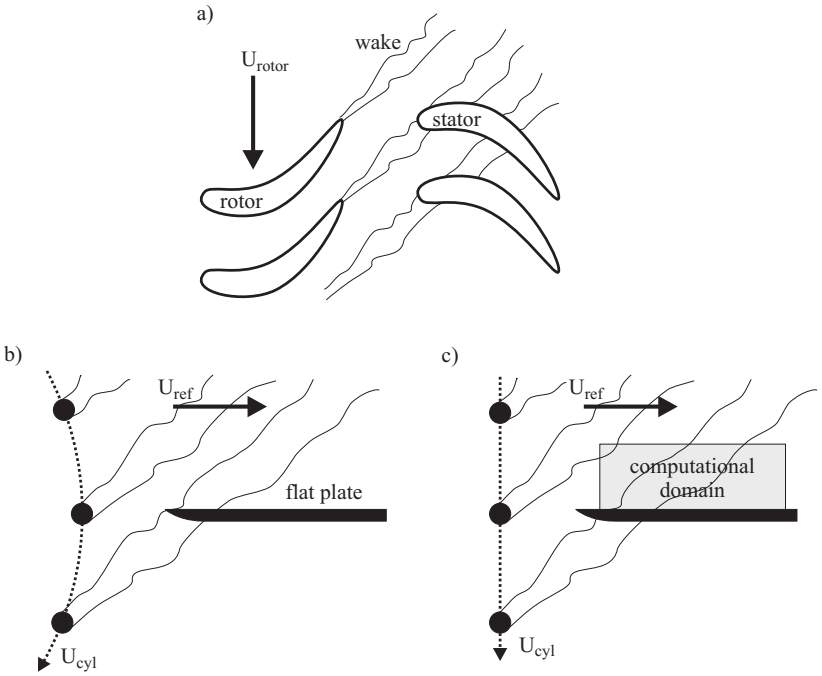

FIGURE 1. a) Schematic of rotor-stator wake interaction; b) layout in the experiments of Liu and Rodi (1991); c) layout in the DNS of Wu *et al.* (1999), and the present LES and RANS.

this case, the transition is referred to as "wake-induced" (Mayle 1991) but still fits under the broader classification of bypass transition (Fig. 1a).

In an effort to remove some of the geometric and physical complexity associated with the turbine cascade, Liu and Rodi (1991) experimentally investigated the wake-induced transition of a flat-plate boundary layer (Fig. 1b). In their experiments, periodic wakes were generated by a series of cylinders mounted on a rotating squirrel cage upstream of the flat plate. In the absence of the periodic wakes, the relatively low Reynolds number and low free-stream turbulence intensity of 0.3% resulted in a laminar boundary layer over the full length of the test plate. With the wakes, they found that transition first occurred in isolated stripes underneath the disturbed free-stream. The stripes traveled downstream and grew together to eventually form a fully turbulent boundary layer. They also found that the streamwise location of this merger moved upstream with increased wake-passing frequency.

The recent DNS of Wu *et al.* (1999) was designed following the experiment of Liu and Rodi (1991) and provided new insights into the mechanisms of bypass transition through a detailed analysis of the calculated flow fields (Fig. 1c). Wu *et al.* found that the transition to turbulence first occurred in isolated spots, which broaden and convect downstream, where they eventually merged with the fully turbulent boundary layer. Analysis of the instantaneous flow field identified long backward jets contained in the fluctuating streamwise velocity field as precursors to turbulent spot formation. They proposed that the backward jets, located near the top of the boundary layer, were associated with a Kelvin-Helmholtz-like inflectional instability that interacts with the free-stream eddies, eventually leading to turbulent spot formation. More recent simulations of bypass tran-

sition under free-stream turbulence (Jacobs and Durbin 2000) also identified backward jets as consistent precursors to turbulent spot formation.

At 52 million and 71 million grid points respectively, the aforementioned transition simulations are some of the largest and most finely resolved ever reported. Interestingly, the bypass transition mechanism they uncovered – the backward jet – is actually a relatively large structure, spanning 100's of wall units in the streamwise direction and about 60 wall units in the spanwise direction. This suggests that a coarser and significantly less expensive LES might be able to capture the bypass transition mechanism.

Yang *et al.* (1994) used LES to study bypass transition of a flat plate boundary layer subject to 5% freestream turbulence intensity. These simulations used the Smagorinsky subgrid scale model modified in an *ad hoc* manner to prevent excessive dissipation in the laminar portion of the boundary layer. They reported good agreement with available experimental data such as the average skin friction coefficient and shape factor, but did not report the resolution of turbulent spots or their precursors. In a more recent LES of natural transition, Huai *et al.* (1997) used the dynamic procedure of Germano *et al.* (1991) to avoid these *ad hoc* modifications. They reported that a localized version (Piomelli and Liu 1995) of the dynamic model gave accurate results both in a statistical sense and in terms of predicting the dynamics of the energy-carrying eddies.

In the present contribution, LES is used to study the wake-induced transition of a flat-plate boundary layer with specific emphasis on the resolution of turbulent spots and their precursors. As a complementary effort, the same problem is simulated using 2-dimensional unsteady RANS. These two results, along with the DNS of Wu *et al.* (1999), represent a truly integrated analysis of this transitional flow and provide a unique opportunity to assess the relative benefits and drawbacks of the various simulation technologies.

2. Governing equations

The tensor equations of motion for the spatially filtered incompressible velocity and pressure fields are given by

$$\frac{\partial \bar{u}_i}{\partial t} + \frac{\partial \bar{u}_j \bar{u}_i}{\partial x_j} = -\frac{\partial \bar{p}}{\partial x_i} + \frac{\partial}{\partial x_j}\left((\nu + \nu_{sgs})\left(\frac{\partial \bar{u}_j}{\partial x_i} + \frac{\partial \bar{u}_i}{\partial x_j}\right)\right) \tag{2.1}$$

$$\frac{\partial \bar{u}_i}{\partial x_i} = 0 \tag{2.2}$$

where the overbar represents spatial filtering on the scale of the grid. Equation (2.1) assumes Boussinesq dynamics to approximate the subgrid stresses, where the subgrid viscosity, ν_{sgs}, is given by the Smagorinsky closure

$$\nu_{sgs} = C\bar{\Delta}^2\sqrt{2\bar{S}_{ij}\bar{S}_{ij}}. \tag{2.3}$$

In equation (2.3), the resolved strain rate tensor is defined

$$\bar{S}_{ij} = \frac{1}{2}\left(\frac{\partial \bar{u}_j}{\partial x_i} + \frac{\partial \bar{u}_i}{\partial x_j}\right), \tag{2.4}$$

and the grid filter width is defined in terms of the local grid spacing

$$\bar{\Delta} = \left(\bar{\Delta}_x \bar{\Delta}_y \bar{\Delta}_z\right)^{1/3}. \tag{2.5}$$

The Smagorinsky constant, C, is calculated using the dynamic procedure of Germano *et al.* (1991) and Lilly (1992) with averaging in the homogeneous direction(s) to avoid the numerical instability associated with large negative C values. In addition, the total viscosity $(\nu + \nu_{sgs})$ is not allowed to be negative.

3. Numerical method

The important role of discrete conservation of mass, momentum, and kinetic energy in obtaining accurate solutions to incompressible turbulent flow problems has been argued by several authors (Morinishi *et al.* 1998, Mittal & Moin 1997). These analyses have considered discrete conservation of the spatial terms as analytical requirements for a proper set of discretized equations. In general, this has meant a staggered arrangement of velocity and pressure and the use of symmetric (central-difference) discretizations for all spatial derivatives. Because of the fractional-step method normally used for time advancement, however, the same conservation requirements cannot be enforced in time. Although the associated errors are generally small and dissipative, the system is not conservative in a discrete sense.

The LES of the present contribution is based on a discretized form of governing Eqs. (2.1) and (2.2) that is 2nd-order accurate and discretely conserves mass, momentum, and kinetic energy (in the inviscid limit) in space and time. The resulting equations closely resemble that given by the 2-level Crank-Nicholson scheme, with a slight modification to the convective term. In the following sections, the conservative discretized equations are introduced, their conservation properties are derived, and the details of their efficient solution is presented.

3.1. *The discretized equations*

Extending the notation of Morinishi *et al.* (1998) to include time, we introduce the following discrete operators for 2nd-order differencing and averaging on a structured orthogonal grid.

$$\left.\frac{\delta_1 \phi}{\delta_1 x_1}\right|_{x_1,x_2,x_3,t} \equiv \frac{\phi\left(x_1 + h_1/2, x_2, x_3, t\right) - \phi\left(x_1 - h_1/2, x_2, x_3, t\right)}{h_1} \tag{3.1}$$

$$\left.\overline{\phi}^{1x_1}\right|_{x_1,x_2,x_3,t} \equiv \frac{\phi\left(x_1 + h_1/2, x_2, x_3, t\right) + \phi\left(x_1 - h_1/2, x_2, x_3, t\right)}{2} \tag{3.2}$$

$$\begin{aligned}\left.\widetilde{\phi\psi}^{1x_1}\right|_{x_1,x_2,x_3,t} \equiv\ & \tfrac{1}{2}\phi\left(x_1 + h_1/2, x_2, x_3, t\right)\psi\left(x_1 - h_1/2, x_2, x_3, t\right) + \\ & \tfrac{1}{2}\psi\left(x_1 + h_1/2, x_2, x_3, t\right)\phi\left(x_1 - h_1/2, x_2, x_3, t\right)\end{aligned} \tag{3.3}$$

In the above equations, ϕ and ψ represent discrete variables that may be cell-centered or staggered, and h_1 is the grid spacing in the x_1 direction. Discrete operators in the x_2, x_3, and t directions are similarly defined. To avoid confusion in the already cumbersome notation of the following sections, the overbar used in Eqs. (2.1) and (2.2) is dropped, and capital letters are used to represent the discrete velocity and pressure fields.

Using this notation, a 2nd-order accurate discretization of continuity equation (2.2) is

$$\frac{\delta_1 U_i}{\delta_1 x_i} = 0. \tag{3.4}$$

Because Eq. (3.4) is in discrete divergence form, it is *a priori* conservative, and we would

expect the scheme to conserve mass locally and globally. Assuming zero viscous and subgrid stresses, a 2nd-order accurate discretization of the momentum equation is

$$\frac{\delta_1 U_i}{\delta_1 t} + \frac{\delta_1 \overline{\overline{U_j}^{1t}}^{1x_i} \overline{\overline{U_i}^{1t}}^{1x_j}}{\delta_1 x_j} + \frac{\delta_1 P}{\delta_1 x_i} = 0. \tag{3.5}$$

Because all terms in Eq. (3.5) are in discrete divergence form (including the time term, if the concept of discrete divergence is extended to time as well), it is *a priori* conservative. Thus, momentum is conserved locally and globally in space and time.

3.2. *Discrete kinetic energy conservation*

As pointed out by Morinishi *et al.* (1998), local kinetic energy cannot be defined unambiguously on the staggered grid because the velocity components are stored at different locations. The required interpolation of velocity components is consistent if we choose the cell center (the location of P) as the location about which to develop the kinetic energy equation.

The vector dot product of the velocity with the momentum equation (3.5) produces the kinetic energy equation which, including the appropriate discrete 2nd-order interpolations, takes the form

$$\overline{U_i}^{1t} \left(\frac{\delta_1 U_i}{\delta_1 t} + \frac{\delta_1 \overline{\overline{U_j}^{1t}}^{1x_i} \overline{\overline{U_i}^{1t}}^{1x_j}}{\delta_1 x_j} + \frac{\delta_1 P}{\delta_1 x_i} \right)^{1x_i} = 0 \tag{3.6}$$

The l.h.s. of (3.6) can be expanded into 3 terms, each of which will be analyzed for conservation separately:

$$(Time) + (Conv.) + (Pres.) = 0. \tag{3.7}$$

Using the identities described by Morinishi *et al.* (1998), the $(Time)$ term can be rearranged as follows

$$(Time) = \overline{\overline{U_i}^{1t} \frac{\delta_1 U_i}{\delta_1 t}}^{1x_i} = \frac{\overline{\delta_1 U_i U_i/2}^{1x_i}}{\delta_1 t} = \frac{\delta_1 \overline{U_i U_i/2}^{1x_i}}{\delta_1 t} = \frac{\delta_1 K}{\delta_1 t} \tag{3.8}$$

where the kinetic energy, K, is defined

$$K = \overline{U_i U_i/2}^{1x_i}. \tag{3.9}$$

Equation (3.8) is in discrete divergence form, and thus the $(Time)$ term of the K equation is conservative. The pressure term can be rearranged as follows

$$(Pres.) = \overline{\overline{U_i}^{1t} \frac{\delta_1 P}{\delta_1 x_i}}^{1x_i} = \frac{\delta_1 \overline{U_i}^{1t} \overline{P}^{1x_i}}{\delta_1 x_i} - P \overline{\frac{\delta_1 U_i}{\delta_1 x_i}}^{1t} \tag{3.10}$$

The first term on the rhs is in divergence form, and the second term involves the discrete continuity equation, which is identically zero. Therefore, the $(Pres.)$ term of the K equation is conservative. Finally, some manipulation of the $(Conv.)$ term yields:

$$(Conv.) = \overline{U_i}^{1t} \frac{\overline{\delta_1 \overline{\overline{U_j}^{1t}}^{1x_i} \overline{\overline{U_i}^{1t}}^{1x_j}}^{1x_i}}{\delta_1 x_j}$$

$$= \frac{1}{2} \frac{\overline{\overline{\overline{U_j}^{1t}}^{1x_i} \widetilde{\overline{U_i}^{1t}} \overline{\overline{U_i}^{1t}}^{1x_j}}^{1x_i}}{\delta_1 x_j} + \frac{1}{2} \overline{U_i}^{1t} \overline{\overline{U_i}^{1t}}^{1t} \overline{\frac{\delta_1 \overline{U_j}^{1t}}{\delta_1 x_j}}^{1x_i} \tag{3.11}$$

The first term on the rhs is in divergence form, and the second term involves the discrete continuity equation, which is identically zero. Therefore the $(Conv.)$ term of the K equation is conservative.

3.3. *Solution procedure*

The coupled, fully-implicit, non-linear system of equations resulting from this choice of discretization can be quite stiff, particularly on the highly stretched grids typical of LES and DNS of wall-bounded shear flows. In the present work, the system is solved iteratively at each time step using algebraic multigrid with smoothing based on the Symmetric Coupled Gauss-Siedel method of Vanka (1986). The system's stiffness is handled by coarsening preferentially in the direction of greatest coefficient strength, a multigrid technique referred to as semi-coarsening (Wesseling 1992). With the judicious selection of coarse grids, it is possible to reduce the maximum residual by 6 orders of magnitude with about 50 workunits per time step (1 workunit is equivalent to one smoothing sweep through the finest grid). Although relatively expensive per time step when compared to the fractional step approximation, the present fully-implicit system is numerically stable for any choice of computational time step, and the discrete conservation properties ensure the method is not dissipative in space and time.

4. Validation: the transitional channel flow

The temporal transition in a channel has been used in the past to demonstrate the performance of the various dynamic models (Germano *et al.* 1991, Meneveau *et al.* 1996). As a validation exercise, the discretely conservative solution method described above was used to solve this flow.

The initial condition consists of a parabolic profile superimposed with a 2-dimensional Tollmien-Schlichting (TS) mode of 2% and a 3-dimensional TS mode of 0.02%. The Reynolds number is 8000 (based on laminar centerline velocity), and the dimensions of the computational domain, normalized by channel half width, are $2\pi \times 2 \times 4\pi/3$ in the streamwise, wall-normal, and spanwise directions respectively. For more details, see Zang *et al.* (1990). As the solution is integrated ahead in time, the TS modes are amplified and the flow undergoes natural transition, leading eventually to fully developed turbulence.

Figure 2 compares the time history of the calculated wall shear stress with that from the DNS of Zang *et al.* (1990). The results for two different grid resolutions are reported. When compared to the DNS result, both LES results capture the characteristic shape of the curve, including the drag crisis. In both cases, the peak wall shear is slightly over-predicted although this has been observed before (Meneveau *et al.* 1996). In the case of the coarse grid simulation, however, the entire transition is significantly delayed. This delay is likely explained by the under-predicted linear amplification rate of the coarse finite differences. Solution of the Orr-Sommerfeld equation using the same wall-normal

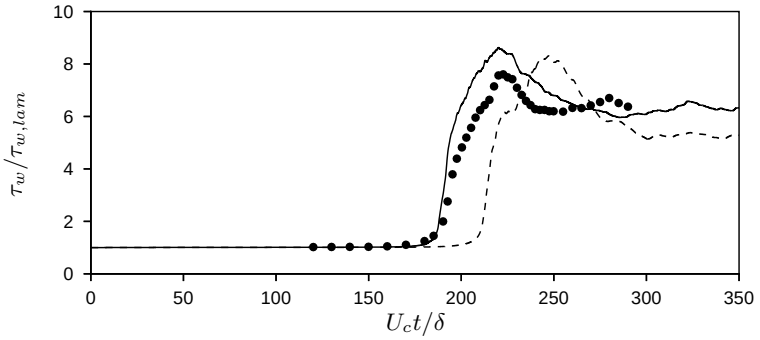

FIGURE 2. Time history of average wall shear stress from the transitional channel simulation. ——— fine LES ($32 \times 128 \times 64$); – – – – coarse LES ($32 \times 64 \times 32$); • DNS of Zang *et al.* (1990)

grid distribution and finite-difference numerics yields an amplification factor (the imaginary part of the eigenvalue) for the imposed 2-dimensional TS mode of $\omega_i = 0.002222$. The "exact" value of $\omega_i = 0.002664$ (Zang & Krist 1989) is higher by a factor of 1.2, corresponding closely to the inverse ratio of the duration of the linear amplification periods of about $220/180 = 1.2$. To show that this should be the case, assume the linear amplification period ends when the amplitude of the imposed 2-dimensional TS mode, ϕ_0, reaches some critical level, ϕ_c. Two different simulations that amplify this mode at different rates will reach the critical amplitude at different times, according to

$$\phi_c = \phi_0 e^{\omega_{i1}\Delta t_1} = \phi_0 e^{\omega_{i2}\Delta t_2}. \tag{4.1}$$

Solving (4.1) for the time ratio yields $\Delta t_1/\Delta t_2 = \omega_{i2}/\omega_{i1}$.

5. Simulation of wake-induced transition

5.1. *Problem definition*

As in Wu *et al.* (1999), the present LES was designed following the experiment of Liu & Rodi (1991). Dimensions were scaled by the characteristic length scale, L, equal to the minimum distance from the upstream cylinders to the leading edge of the flat plate. Velocities were scaled by characteristic velocity scale U_{ref}, the freestream velocity in the absence of wakes. The problem Reynolds number was $Re = U_{ref}L/\nu = 1.5 \times 10^5$. The downward velocity of cylinders was $U_{cyl}/U_{ref} = 0.7$, and the passing wake period was $T = 1.67L/U_{ref}$, corresponding to case number 4 in the experiments of Liu & Rodi (1991).

5.2. *Boundary conditions*

The application of boundary conditions followed the procedure described in Wu *et al.* (1999) with one exception: the precomputation of the self-similar plane wake used as the inlet condition was appropriately filtered for the coarser grid spacing of the present simulation.

5.3. *Computational domain*

Figure 1c schematically illustrates the computational domain used in the present LES. In an effort to minimize the problem size, the domain selected was only a fraction of the

DNS domain of Wu *et al.* (1999). In the streamwise direction, the domain was shortened to just include the transition, $0.1 < x/L < 1.75$. In the spanwise direction, the domain width was $0 < z/L < 0.1$, and in the wall-normal direction, $0 < y/L < 0.3$.

5.4. *Grid spacing and time step*

The grid spacing requirements for accurate DNS of bypass transition have been well established through grid independence studies performed as a part of recent simulations. For the bypass transition simulations of Jacobs & Durbin (2000), the grid spacing (based on maximum friction velocity) was $\Delta x^+ = 11.7$, $\Delta z^+ = 6.0$. This is in agreement with the earlier recommendations of Rai & Moin (1993). The DNS of Wu *et al.* (1999) used a slightly coarser spacing of $\Delta x^+ = 24$, $\Delta z^+ = 11$ (based on friction velocity at $x = 3$).

The grid spacing requirements for accurate LES of bypass transition, however, are less well established. In the bypass transition LES of Yang *et al.* (1994), the grid spacing was $\Delta x^+ = 80$ and $\Delta z^+ = 14$. Based on the experience gained through the present research, we believe this streamwise spacing to be too coarse to resolve discrete turbulent spots. In the present work, the finest grid size used was $256 \times 64 \times 48$, which corresponded to a grid spacing based on maximum friction velocity of $\Delta x^+ = 45$ and $\Delta z^+ = 17$. In the wall-normal direction, spacing at the wall was $\Delta y^+ = 2$.

The computational time step was set constant at $\Delta t = 0.003 L/U_{ref}$, which corresponded to a time step in wall units (based on maximum friction velocity) of $\Delta t^+ = \Delta t u_\tau^2/\nu = 1.3$.

5.5. *Computational details*

The combination of reduced domain size, increased grid spacing, and increased computational time step yielded a reduction in problem size by a factor of about 160 relative to the DNS. Computations were carried out on a parallel PC cluster at the University of Waterloo. Simulations were typically run for 10 wake passing periods (about 5500 time steps), and required about 3 days using 32 nodes of the cluster.

6. Results

6.1. *Instantaneous fields*

The relatively small size of the present LES (about 700,000 grid points) afforded some experimentation with the grid spacing. The first simulations were performed on relatively coarse grids with $\Delta x^+ = 95$ and $\Delta z^+ = 35$. Although transition was observed to occur at approximately the correct location (when compared to the DNS), inspection of the instantaneous velocity fields did not reveal isolated turbulent spots. Further, the spanwise resolution in these coarse simulations was certainly not capable of properly resolving the backward jet structures, which appear to have a width of about 60 wall units.

6.1.1. *Turbulent spots*

In the finest LES, however, distinct turbulent spots were clearly discernible. Figure 3 uses the fluctuating velocities in the wall normal direction at 5 equally spaced times to visualize the transition. The interaction between the passing wake and the laminar boundary layer appears as elongated puffs at $t/T = 0$, but breakdown to a turbulent spot does not occur until some time closer to $t/T = 0.4$. At $t/T = 0.4$, the isolated spot is clearly discernible with its characteristic arrowhead pointing upstream. As the turbulent spot is convected downstream, it grows and eventually merges with the fully turbulent portion of the boundary layer.

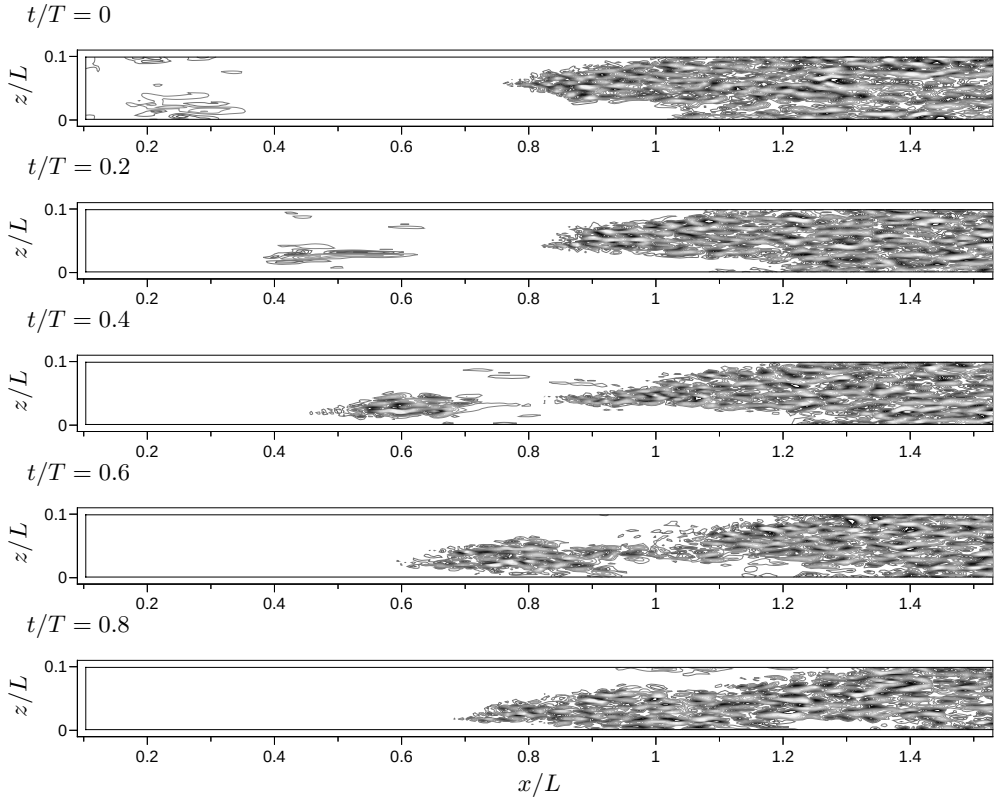

FIGURE 3. Visualization of turbulent spot formation and growth using v-component of fluctuating velocity in the x-z plane near the wall ($y/\delta_{99} = 0.4$ at $x/L = 0.8$). Contours represent $-0.1 < v/U_{ref} < 0.1$ in 0.01 increments.

While qualitatively similar to the DNS result, the following important differences are noted:

(1) The front separating the laminar and fully turbulent portion of the boundary layer is much more irregular in the LES, with long fingers of turbulence reaching significantly upstream. These fingers are thin in the spanwise direction but do not dissipate or convect downstream with the rest of the boundary layer when not being fed by spots.

(2) In the LES, the streamwise location at which the turbulent spots merge with the fully turbulent portion of the boundary layer is in the range of $x = 1$ to 1.2. In the DNS, this location was further downstream at $x = 1.5$ to 1.7.

(3) Close inspection of the turbulent spot reveals the presence of $2 - \Delta$ fluctuations in the velocity field near the upstream edge, indicating under-resolution in the streamwise direction particularly.

6.1.2. *Backward jets*

The backward jet structures observed in the DNS as consistent precursors to turbulent spot formation were also resolved by the LES. By saving restart files regularly, it was possible to stop the simulation when a turbulent spot was identified and restart at an earlier time to look for evidence of spot precursors. Figure 4a) plots the fluctuating velocity vectors in the $x - z$ plane at an elevation near the top of the boundary layer just

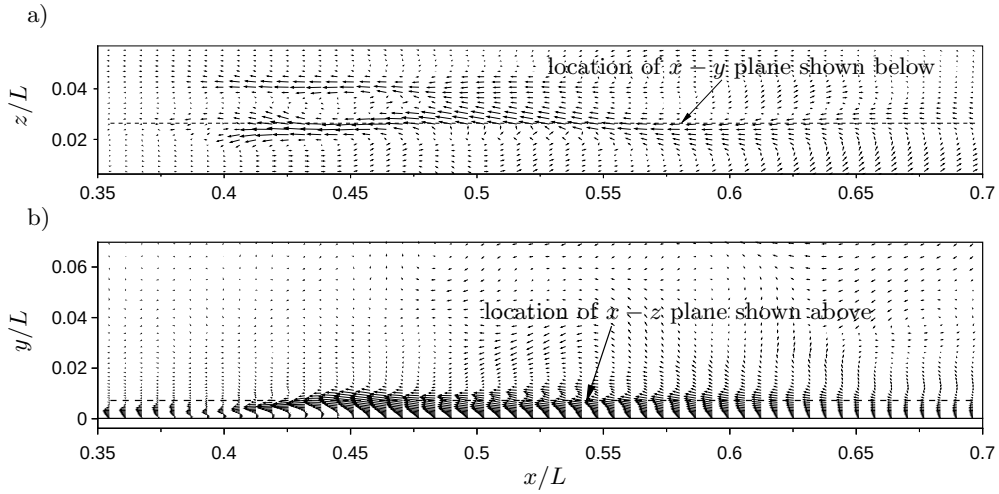

FIGURE 4. Fluctuating velocity vectors upstream of a future turbulent spot showing backward jet structure. a) $x-z$ plane; b) $x-y$ plane.

prior to the appearance of the turbulent spot visualized in Fig. 3. A strong backward jet is evident. The spanwise width of the jet is about 80 wall units, similar to those seen in the bypass transition DNS of Jacobs & Durbin (2000). Figure 4b) shows the fluctuating velocity vectors of the same jet through the $x-y$ plane.

6.2. *Average quantities*

To make our investigation of this transitional flow more comprehensive, unsteady RANS simulations were also performed. These simulations used the STREAM code of Lien & Leschziner (1994), and the v^2-f turbulence model of Lien & Durbin (1996). Computing time per simulation was approximately 2 hours on a desktop PC. This represents a reduction in computational effort of about 2 orders of magnitude compared to the LES.

Figure 5 compares the average skin friction calculated by the LES and RANS to the DNS of Wu *et al.* (1999). Both the LES and RANS correctly predict the onset of transition. In the case of the LES, however, the transition length is under-predicted. This is consistent with the observation that the turbulent spots merge with the fully turbulent boundary layer further upstream than in the DNS. There are several possible explanations for this although the most compelling is that the dissipation rate given by the standard dynamic model is simply too low in the transition region, where the spanwise averaging used in calculating the model constant includes significant regions of laminar flow. This explanation suggests that another incarnation of the dynamic model might be more appropriate for modeling this type of transitional flow even when a homogeneous direction is present such as the dynamic localization model of Ghosal *et al.* (1995) or the Lagrangian dynamic model of Meneveau *et al.* (1996).

The transition length predicted by RANS agrees with the DNS result although the overshoot of average skin friction relative to the flat plate correlation (seen in both the DNS and present LES) is not observed. No tuning of model constants for this particular flow was done.

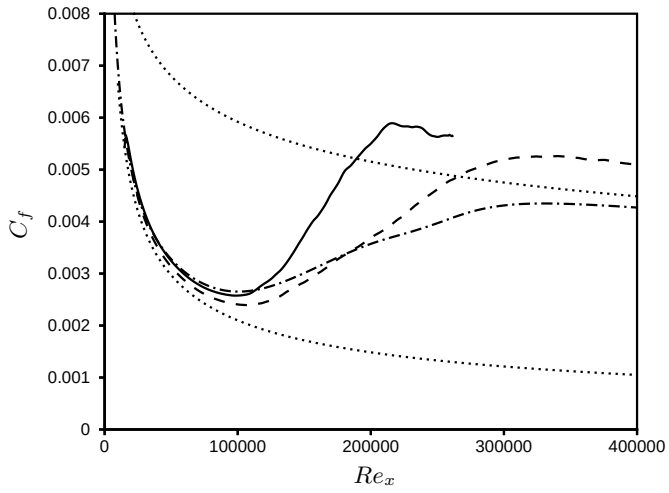

FIGURE 5. Comparison of time averaged skin friction coefficient along flat plate, ——— LES; —·— RANS; – – – DNS of Wu *et al.* (1999); ····· laminar and turbulent correlations.

7. Conclusions

LES and unsteady RANS simulations have been made of a spatially-evolving flat-plate boundary-layer undergoing transition induced by periodically passing wakes. The LES used a novel kinetic-energy conserving finite-volume discretization of the incompressible Navier-Stokes equations and the standard dynamic Smagorinsky subgrid-scale model. RANS simulations were based on the STREAM code of Lien & Leschziner (1994) with the $v^2 - f$ turbulence model of Lien & Durbin (1996).

Overall, RANS and LES both have benefits when applied to this flow. RANS predicts a slightly superior average skin friction coefficient at enormously reduced computational cost although the performance under more complex conditions (for example, flow in a turbine cascade involving complex geometry, higher freestream turbulence intensity, and pressure gradients) remains to be tested.

The LES was able to resolve both turbulent spots and their backward jet precursors, consistent with the recent DNS results of Wu *et al.* (1999) and Jacobs & Durbin (2000). The location of the onset of transition agreed with the DNS result; however, the transition length was under-predicted. This discrepancy may be related to the spanwise averaging used in the calculation of the subgrid scale model coefficient, and other implementations of the dynamic model might give superior results. The potential improvement from these other models remains to be tested and is the subject of ongoing research.

Acknowledgment

The authors are grateful to U. Piomelli for providing the initial condition for the transitional channel simulations.

REFERENCES

Germano, M., Piomelli, U., Moin, P., & Cabot, W. H. 1991 A dynamic subgrid-scale eddy viscosity model. *Phys. Fluids A.* **3**, no. 7, 1760-1765.

Ghosal, S., Lund, T. S., Moin, P. & Askelvoll, K. 1995 A dynamic localization model for large-eddy simulation of turbulent flows. *J. Fluid Mech.* **286**, 229-255.

Huai, X., Joslin, R. D. & Piomelli, U. 1997 Large-eddy simulation of transition to turbulence in boundary layers. *Theoret. Comput. Fluid Dyn.* **9**, 149-163.

Jacobs, R. G., & Durbin, P. A. 2000 Simulations of bypass transition. *J. Fluid Mech.*, to appear.

Lien, F. S. & Durbin, P. A. 1996 Non-linear $k - \epsilon - v^2$ modeling with application to high lift. *1996 Summer Program Proceedings,* Center for Turbulence Research, NASA Ames/Stanford Univ. 5-22.

Lien, F. S. & Leschziner, M. A. 1994 A general non-orthogonal collocated FV algorithm for turbulent flow at all speeds incorporating second-moment closure. *Comp. Meth. Appl. Mech. Eng.* **114**, 123-167.

Lilly, D. K. 1992 A proposed modification of the Germano subgrid scale closure method. *Phys. Fluids A.* **4**(3), 633-635.

Liu, X. & Rodi, W. 1991 Experiments on transitional boundary layers with wake-induced unsteadiness. *J. Fluid Mech.* **231**, 229-256.

Mayle, R. E. 1991 The role of laminar-turbulent transition in gas turbine engines. *ASME J. of Turbomachinery* **113**, 509-537.

Meneveau, C., Lund, T. S. & Cabot, W. H. 1996 A Lagrangian dynamic sungrid-scale model of turbulence. *J. Fluid Mech.* **319**, 353-385.

Mittal, R. & Moin, P. 1997 Suitability of upwind-biased finite difference schemes for large-eddy simulation of turbulent flows. *AIAA J.* **35**(8), 1415-1417.

Morinishi, Y., Lund, T. S., Vasilyev, O. V. & Moin, P. 1998 Fully conservative higher order finite difference schemes for incompressible flow. *J. Comput. Phys.* **143**, 90-124.

Piomelli, U. & Liu, J. 1995 Large eddy simulation of rotating channel flows using a localized dynamic model. *Phys. Fluids A.* **7**, 839.

Rai, M. M. & Moin, P. 1993 Direct numerical simulation of transition and turbulence in a spatially evolving boundary layer. *J. Comput. Phys.* **109**, 169-192.

Vanka, S. P. 1986 A calculation procedure for three-dimensional steady recirculating flows using multigrid methods. *Comp. Meth. Appl. Mech. Eng.* **55**, 321-338.

Wessling, P. 1992 An Introduction to Multigrid Methods. John Wiley and Sons.

Wu, X., Jacobs, R. G., Hunt, J. C. R. & Durbin, P. A. 1999 Simulation of boundary layer transition induced by periodically passing wakes. *J. Fluid Mech.* **398**, 109-154.

Yang, Z., Voke, P. R. & Savill, M. A. 1994 Mechanisms and models of boundary layer receptivity deduced from large-eddy simulation of by-pass transition. Direct and large-eddy simulation I, P. R. Voke *et al.* (eds.), Kluwer Academic, Dordrecht, 225-236.

Zang, T. A., Gilbert, N. & Kleiser, L. 1990 Direct numerical simulation of the transitional zone. Instability and Transition, M. Y. Hussaini & R. G. Voigt (eds.), Springer-Verlag, New York, 283-299.

Zang, T. A. & Krist, S. E. 1989 Numerical experiments on stability and transition in plane channel flow. *Theoret. Comput. Fluid Dyn.* **1**, 41-64.